

Acid-Promoter-Free Ethylene Methoxycarbonylation over Ru-Clusters/Ceria: The Catalysis of Interfacial Lewis Acid–Base Pair

Jinghua An,^{†,‡,⊥} Yehong Wang,^{†,⊥} Jianmin Lu,^{†,⊥} Jian Zhang,[†] Zhixin Zhang,[†] Shutao Xu,[†] Xiaoyan Liu,[†] Tao Zhang,[†] Martin Gocyla,[§] Marc Heggen,[§] Rafal E. Dunin-Borkowski,[§] Paolo Fornasiero,^{||} and Feng Wang^{*,†,⊥}

[†]State Key Laboratory of Catalysis, Dalian National Laboratory for Clean Energy, Dalian Institute of Chemical Physics, Chinese Academy of Sciences, 457 Zhongshan Road, Dalian 116023, China

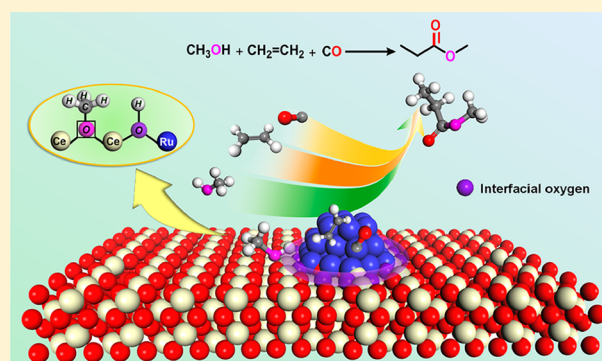
[‡]University of Chinese Academy of Sciences, Beijing 100049, China

[§]Ernst Ruska Centre for Microscopy and Spectroscopy with Electrons and Peter Grünberg Institute, Forschungszentrum Juelich GmbH, Juelich 52425, Germany

^{||}Department of Chemical and Pharmaceutical Sciences, INSTM, Center of Excellence for Nanostructured Materials (CENMAT), University of Trieste, Via L. Giorgieri 1, Trieste 34127, Italy

Supporting Information

ABSTRACT: The interface of metal-oxide plays pivotal roles in catalytic reactions, but its catalytic function is still not clear. In this study, we report the high activity of nanostructured Ru/ceria (Ru-clusters/ceria) in the ethylene methoxycarbonylation (EMC) reaction in the absence of acid promoter. The catalyst offers 92% yield of MP with TOF of 8666 h⁻¹, which is about 2.5 times of homogeneous Pd catalyst (~3500 h⁻¹). The interfacial Lewis acid–base pair [Ru–O–Ce–Vö], which consists of acidic Ce–Vö (oxygen vacancy) site and basic interfacial oxygen of Ru–O–Ce linkage, acts as active site for the dissociation of methanol and the subsequent transfer of hydrogen to the activated ethylene, which is the key step in acid-promoter-free EMC reaction. The combination of ¹H MAS NMR, pyridine-IR and DFT calculations reveals the hydrogen species derived from methanol contains Brönsted acidity. The EMC reaction mechanism under acid-promoter-free condition over Ru-clusters/ceria catalyst is discussed.



1. INTRODUCTION

Metal oxide catalysts have been widely used in the industry of petrochemical, fine chemical and environmental industry.¹ Interface between nano- or subnano-sized metal particles and their oxide supports has profound effects on the stability, activity and selectivity of heterogeneous catalysts.² Model studies on metal-oxide catalysis have provided deep insights into the interfacial structure of metal-oxide down to the atomic level, and have shed light onto many catalytic processes.^{1a,3} Particularly they disclose that the catalytic reactions are related to coordinately unsaturated metal sites at exposed metal-oxide perimeters, which can accommodate O₂ or CO adsorption and activation.⁴ Very recently, Hu and co-workers have found that the interfacial sites of FeO/Pt(111) are responsible for methanol oxidation to formaldehyde by DFT calculations.⁵ This study has demonstrated that the interfacial oxygen significantly reduces the O–H cleavage barrier of methanol to below 0.1 eV. In addition, Li and co-workers have found that the interfacial oxygens (metal^I–oxygen–metal^{II}) on FeO/Pt(111) and Cu₂O/Ag(111) are important for achieving high activity in benzyl alcohol oxidation through STM and DFT

calculations.^{1a} Although tremendous advances have been achieved on the interfacial catalysis on metal sites,⁶ little attention has been paid to the role of interfacial acid–base catalysis of metal-oxide systems. Actually, the interfacial acid–base catalysis should be considered particularly when oxides are used as major components, additives or supports.

Catalysis by ceria is mostly driven by its ability to store and release oxygen because of the facile redox cycle of the cerium ions (Ce⁴⁺ ↔ Ce³⁺).⁷ As such, ceria is a key catalyst in three-way catalytic converters,^{7c} water–gas shift reaction,⁸ CO oxidation,⁹ methane combustion and complex organic reactions.^{1b,4a–c,10} The introduction of other metals to ceria usually decreases the formation energy of oxygen vacancy (Vö) and leads to unique catalytic activity.^{10h,11} This enables the ceria-based catalysts to be potentially employed as multifunctional catalysts in complex reaction system.

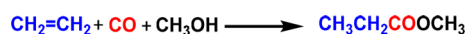
Alkoxy carbonylation of olefins with carbon monoxide (CO) and alcohols is an atomic-economic C–C and C–O bond

Received: February 12, 2018

Published: February 26, 2018

formation reaction.¹² Methyl propionate (MP) is a key precursor in the synthesis of methyl methacrylate (MMA), a monomer for poly methyl methacrylate (PMMA) that is a highly demanded transparent thermoplastic.¹³ Synthesis of MP from three low-carbon building blocks, i.e., ethylene, CO and methanol, is an ideal route as the three feedstocks can be obtained from fossil or renewable sources.¹⁴ However, the reaction requires multiple active sites and promoters to assemble three molecules to one by forming new bonds. So far, Pd-phosphine complexes catalysts with acid promoters are mostly used in the ethylene methoxycarbonylation (EMC) reaction (Scheme 1).^{13,15} However, the catalytic systems

Scheme 1. Synthesis of Methyl Propionate (MP) from Three Low-Carbon Building Blocks (Ethylene, CO and Methanol) via the EMC Reaction



require mineral acids as promoters, such as sulfuric acids.^{12,13,16} Beller and co-workers have reported seminal works on Pd(OAc)₂ catalyst with sulfonic acids as promoters in the EMC reaction. They found the catalytic activity could be promoted by placing pyridine group in phosphor-contained ligands, where the nitrogen of pyridine was considered to be a weak basic site for methanol proton transfer.¹⁷ Rüsager and co-workers have reported acidic ionic liquids function as both reaction media and acid promoters in the EMC reaction.¹⁸ NMR investigations have shown that the protonated phosphine is formed through the reaction between free ligand and in situ generated HCl, evidencing the formation of the Pd hydride species under the reaction conditions.¹⁸

Previous studies have shown that either preadded acid promoters or in situ generated HCl is indispensable for the EMC reaction. The known reaction mechanism suggests the acid promoter is required to preserve catalytic activity of Pd-complexes by generating and stabilizing Pd hydride species. However, from an industrial point of view, the use of acid promoters will raise the issue of the reaction vessel corrosion and the product separation. We conceived that if a catalyst could generate Brønsted acid sites from a convenient hydrogen donor, it is unnecessary to use mineral acids in the EMC reaction.

We herein report the synthesis of MP via the EMC reaction over Ru-clusters/ceria catalyst under acid-promoter-free condition. Methanol acts as hydrogen donor, reactant and solvent. The catalyst offers 92% yield of MP, which gives 2.5 times higher of TOF value than the homogeneous Pd systems. The unexpected good performance of the catalyst is due to its suitable spatial and electronic structure. HR-TEM reveals the highly dispersed Ru clusters on ceria. The combination of in situ XPS, XANES/EXAFS and other characterizations proves the presence of Lewis acid–base pair [Ru–O–Ce–V_o], verified by ¹H MAS NMR, DFT and pyridine-IR, at the interface of Ru and ceria. Methanol is dissociated to methoxyl and hydrogen species at Ce–V_o site. And then the hydrogen species transferred to the activated ethylene through the interfacial oxygen of Ru–O–Ce. The weak binding of interfacial oxygen makes the hydrogen act as Brønsted acid, which can avoid the addition of mineral acids that are used in the homogeneous systems.

2. EXPERIMENTAL SECTION

Chemicals and Reagents. All chemicals are of analytical grade and used as purchased without further purification. Most of the chemicals are purchased from J&K Chemicals and Aladdin Chemicals, except Noble metals salt (the Non Ferrous Metal Institute of Shenyang) and NH₄OH (Damao Chemical Reagent Factory China). The detail list of these chemicals and the reagents are shown in Table S1.

Catalyst Preparation. Ceria nanoparticles were prepared by a precipitation method used in our previous studies.¹⁹ Nanostructured ceria with various shapes (rod, cube, and octahedron) were prepared by the hydrothermal method according to the literature reports.²⁰ The Ru/ceria catalyst was prepared by a wet impregnation method. 5.0 g of ceria was added into a 30 mL solution of RuCl₃ containing 0.1 g of Ru, and stirred slowly for 20 h at room temperature. The slurry was then dried at 120 °C in an oven and calcined at 200 °C. The dried solid was reduced at 350 °C in H₂ (30 mL·min⁻¹) for 4 h. Other Ru/ceria catalysts reduced at various temperatures were prepared for comparison and marked as Ru/ceria-T (°C), such as Ru/ceria-150 °C. The same impregnation procedure was employed for other oxides-supported Ru catalysts. The content of Ru in all mentioned catalysts was 2 wt % relative to oxide supports.

Catalytic Reactions and Product Analyses. The catalyst, methanol (4.0 mL) and a magnetic stir bar were loaded into a Teflon-lined autoclave reactor, respectively. The reactor was purged with ethylene (99.9% purity, Dalian Guangming Special Gas Products Co., Ltd.) for three times. Then, ethylene and CO (99.9%, Kena Co., Ltd.) were charged into the reactor to a certain pressure. Then, the reactor was sealed and placed in a preheated mantle at the desired temperature. Further care has to be taken as CO is a colorless, odorless, and tasteless but highly toxic gas.²¹ After reaction, products were collected and analyzed by gas chromatography–mass spectrometry (GC-MS) using an Agilent 7890A/5975C instrument equipped with an HP-5 MS column (30 m in length, 0.25 mm in diameter). The yield of MP was determined by GC and calculated based on ethylene.

Characterizations of Catalysts. The microstructures of catalysts were examined by TEM using a JEOL JEM-2000EX and a FEI Tecnai G2 F30 S-Twin. HAADF-STEM was performed using an FEI Titan 80–200 (ChemSTEM).²² These facilities were located at Ernst Ruska Centre for Microscopy and Spectroscopy with Electrons and Peter Grünberg Institute (Forschungszentrum Juelich GmbH, Juelich, Germany). Electron microscope was operated at 200 kV, equipped with a spherical-aberration (Cs) probe corrector (CEOS GmbH), and a high-angle annular dark field detector. A probe semiangle of 25 mrad and an inner collection semiangle of the detector of 88 mrad were used. Compositional maps were obtained with energy-dispersive X-ray spectroscopy (EDX) using four large-solid-angle symmetrical Si drift detectors. For EDX analysis, Ru L and Ce L peaks were used. High resolution transmission electron microscopy (HRTEM) investigations were performed using an FEI-Titan 80–300 electron microscope equipped with a Cs corrector for the objective lens.²³ The microscope was operated at a voltage of 300 kV using the negative-Cs imaging technique (NCSEI, with Cs set at around ~13 μm and defocus around +6 nm). In situ IR spectra were collected on a Bruker Tensor 27 instrument. The catalyst was pressed into a self-supporting disk (13 mm in diameter) and placed into an IR cell. Prior to the adsorption of probe molecule (ethylene, CO, methanol or pyridine), the sample disk was reduced at 350 °C for 1 h in H₂ flow (30 mL·min⁻¹) and then cooled down to room temperature. Subsequently, the IR cell with catalyst disk was pumped down to <6 × 10⁻³ Pa and a spectrum was recorded as the background. Then, the probe molecule was introduced to the IR cell for the adsorption. For the adsorption of ethylene, ethylene was introduced to IR cell and remained at 0.4 MPa for 30 min and then desorbed by vacuum pumping for 30 min. Each spectrum was collected after cooling down to room temperature. For the adsorption of methanol, methanol was introduced into the cell by flowing Ar gas through a methanol bubbler. The catalyst disk was exposed to methanol vapor at room temperature for 30 min. IR spectrum of the chemisorbed methanol was recorded at room

Table 1. EMC Reaction over Various Catalysts^a

| entry | catalyst | selectivity (%) ^b | | | yield of MP (%) |
|-----------------|---------------------|------------------------------|-----|-----|-----------------|
| | | MP | DMP | PTO | |
| 1 | Ru/ceria-RT | 95 | 4 | 1 | 39 |
| 2 | Ru/ceria-150 °C | 93 | 4 | 3 | 39 |
| 3 | Ru/ceria-250 °C | 95 | 4 | 1 | 37 |
| 4 | Ru/ceria-350 °C | 97 | 1 | 2 | 53 |
| 5 | Ru/ceria-450 °C | 94 | 4 | 1 | 35 |
| 6 | Ru/TiO ₂ | >99 | 0 | 0 | 20 |
| 7 | Ru/WO ₃ | >99 | 0 | 0 | 12 |
| 8 | Ru/NiO | 0 | 0 | 0 | 0 |
| 9 | Ru/MoO ₃ | 0 | 0 | 0 | 0 |
| 10 | Ru/ZrO ₂ | >99 | 0 | 0 | 6 |
| 11 | Ru/SiO ₂ | >99 | 0 | 0 | 7 |
| 12 | Ru/MgO | >99 | 0 | 0 | 8 |
| 13 | ceria | 0 | 0 | 0 | 0 |
| 14 | no catalyst | 0 | 0 | 0 | 0 |
| 15 ^c | Ru/ceria | 0 | 0 | 0 | 0 |
| 16 ^d | RuCl ₃ | 74 | 5 | 21 | 16 |
| 17 | Ru/ceria-rod | 94 | 4 | 2 | 55 |
| 18 | Ru/ceria-cube | 92 | 2 | 6 | 51 |
| 19 | Ru/ceria-octahedron | 95 | 2 | 1 | 45 |

^aReaction conditions: catalyst (0.15 g), ethylene (7.5 mmol), CO (0.9 MPa), methanol (4 mL), 165 °C, 6 h. MP yield is calculated based on ethylene. ^bSelectivity is determined by integrating GC peak area since the major product is MP. ^cIn the absence of CO. ^dRuCl₃ (0.03 mmol), ethylene (7.5 mmol), CO (0.9 MPa), methanol (4 mL), 165 °C, 12 h.

temperature. For the adsorption of CO, the catalyst disk was exposed to CO at room temperature for 30 min first. Then, the IR cell with catalyst disk was charged with flowing Ar gas (50 mL·min⁻¹) at room temperature for 30 min. IR spectrum of the chemisorbed CO was recorded at room temperature. For the adsorption of pyridine to detect the acidity, pyridine vapor was introduced into the system and then desorbed at different temperatures ranging from room temperature to 350 °C. Each spectrum was collected after cooling down to room temperature. For the detection of acidity of ceria or Ru/ceria after methanol preadsorption, the catalyst disk was exposed to methanol vapor first. And then methanol was desorbed at room temperature. After that, pyridine vapor was introduced into the system and desorbed at different temperatures ranging from room temperature to 350 °C. Each spectrum was collected after cooling down to room temperature. In situ FT-IR was also applied in tracking the EMC reaction of ethylene, CO and methanol over Ru/ceria. Ethylene, CO and methanol were introduced to the IR cell with a total pressure of 0.4 MPa for 30 min. Then, the catalyst was treated at a desired temperature for 30 min and then desorbed by vacuum pumping for 30 min. Each spectrum was recorded after cooling down to room temperature. In situ X-ray photoelectron spectroscopy (XPS) analysis was performed using an ESCALAB250Xi (Thermo, USA), equipped with an Al K α (1486.6 eV) as the exciting source. First, the catalyst was pressed into the wafers, degassed under vacuum and then put into the analysis chamber for detection before reduction. Then high purity H₂ (99.999%) was flowed into the chamber and heated to the set temperatures ranging from room temperature to 450 °C (room temperature, 150, 250, 350 and 450 °C) for 1 h. Spectra were started to be collected after cooling to room temperature in high vacuum (1 × 10⁻⁸ Pa). The Ru^{δ+}/Ru⁰ ratio (molar ratio of surface atoms) was calculated according to the following eq 1.²⁴

$$\frac{n_i}{n_j} = \frac{I_i}{I_j} \times \frac{\sigma_j}{\sigma_i} \times \frac{E_{k_j}^{0.5}}{E_{k_i}^{0.5}} \quad (1)$$

where i : Ru^{δ+} species; j : Ru⁰ species; n : the numbers of surface Ru atom; I : the intensity of XPS, peak area; σ : photoionization cross-

section; $AlK\alpha$: Ru 3d_{5/2} = 7.39; E_k : photoelectron kinetic energy, $E_k = h\nu - BE$ ($AlK\alpha$, $h\nu = 1486.6$ eV).²⁵ XANES and EXAFS spectra at Ru K-edge were collected at the BL14W1 at the Shanghai Synchrotron Radiation Facility (SSRF), Shanghai, China. An energy selection was undertaken with a double Si(311)-crystal monochromator. A Ru foil was used for the energy calibration. Before experiments, all the samples were reduced at 350 °C in H₂ for 4 h and sealed in Kapton film to avoid exposure to air. The spectra were recorded at room temperature under transmission mode. The Athena software package was used to analyze the data. ¹H MAS NMR spectra were collected on a Bruker Avance III 600 MHz spectrometer at room temperature using a 4 mm low-gamma probe. In a typical ¹H MAS NMR experiment for methanol adsorption, 200 mg of dried sample material was placed in a quartz tube and reduced in flowing H₂ (20 mL·min⁻¹) at 350 °C for 30 min. Then it was cooled down to room temperature after purging with flowing He gas (20 mL·min⁻¹) for 30 min. Subsequently, the sample was exposed to methanol vapor, which was introduced by flowing He gas (20 mL·min⁻¹) through a methanol bubbler into the cell. Finally, the sample was transferred to an NMR rotor for ¹H MAS NMR spectra acquisition. ¹H MAS NMR of methanol and ethylene coadsorption was also collected. The sample was exposed to methanol vapor and ethylene. Methanol vapor was introduced by flowing ethylene gas (20 mL·min⁻¹) through a methanol bubbler into the cell. Finally, the sample was transferred to an NMR rotor for ¹H MAS NMR spectra acquisition. The general characterizations such as XRD, TPD and Raman were also conducted and the experimental details were shown in Supporting Information.

DFT Calculations. All DFT calculations were performed using periodic plane wave based density functional theory program VASP (Vienna Ab Initio Simulation Package).²⁶ The exchange correlation functional was described within the generalized gradient approximation by the Perdew–Burke–Ernzerhof formulation (GGA-PBE).²⁷ The electron–ion interactions were treated by the projector-augmented wave method (PAW).²⁸ The kinetic energy cutoff of the plane-wave basis sets was fixed to 400 eV for all calculations. The 1s valence electron of H, 2s²2p² of C, 2s²2p⁴ of O, 4d⁷5s¹ of Ru, and 5s²5p⁶4f¹5d¹6s² of Ce were explicitly considered. All self-consistent

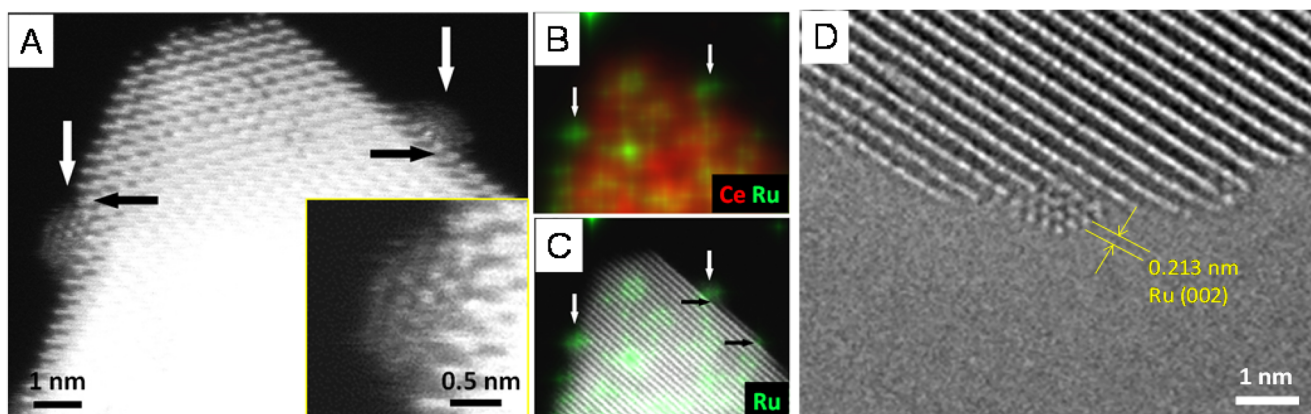


Figure 1. (A) HAADF-STEM images, (B) EDX elemental mapping, and (C) combined HAADF-STEM image and EDX elemental mapping of Ru clusters (white arrows) on ceria. The inset in (A) show enlarged images of the Ru clusters. (D) HRTEM image under NCSI conditions of a Ru cluster on ceria substrate showing the lattice spacing of Ru (002).

field calculations were converged to 1×10^{-5} kJ·mol⁻¹. DFT+U corrections were employed to mitigate the self-interaction errors for Ce with the value of $U-J = 5.0$ eV. The DFT-D3 methodology by Grimme and co-workers²⁹ was used to include the corrections for dispersion interactions. All atomic coordinates of the Ru clusters, put in the cubic box with a side length of 20 Ångstroms, were fully relaxed to a force of <0.02 eV·Å⁻¹ on each atom. A Brillouin zone integration was performed using the Γ point only and a Gaussian smearing width of 0.05 eV. The lattice constant of bulk CeO₂ was optimized to be 5.479 Å in reasonable agreement with the experimental value ($a = 5.411$ Å). This lattice constant was then used to construct a periodic CeO₂ (110) $p(2 \times 3)$ slab with 9 atomic layers (which are equal to 3 stoichiometric layers) separated by a vacuum layer of 15 Å to eliminate interactions between the slab and its periodic images. In total, there were 27 Ce atoms and 54 O atoms in the slab. The bottom 4 atomic layers were fixed to their optimized bulk configuration during all computations, and the top 5 atomic layers and surface intermediates were fully relaxed. All atomic coordinates of the adsorbates and the atoms in the relaxed layers were optimized to a force of <0.02 eV·Å⁻¹ on each atom. Brillouin zone integration was performed using a $3 \times 4 \times 1$ Monkhorst–Pack grid and a Gaussian smearing width of 0.05 eV. The transition state of each elementary reaction step was located by a combination of the nudged elastic band (NEB) method³⁰ and the dimer method.³¹ In the NEB method, the path between the reactant(s) and product(s) was discretized into a series of 5 structural images. After the NEB calculation, the image which was closest to a likely transition state structure was later employed as an initial guess structure for the dimer method.

3. RESULTS AND DISCUSSION

Catalyst Screening Tests in the EMC Reaction and Optimization of the Reaction Conditions. We previously found that Ru/ceria (nanoparticle) showed excellent catalytic performance in the carbonylation of amines to formamides.³² Ru catalysts are also reported in CO activation reactions.³³ Thus, we first used Ru/ceria in the EMC reaction to synthesize MP in methanol in a batch reactor. Meanwhile, the effect of reducing temperature on the Ru/ceria performance was investigated (Table 1, entries 1–5). The results suggest that Ru/ceria reduced at 350 °C exhibited the best catalytic activity with 53% MP yield (Table 1, entry 4) with less than 3% of pentan-3-one (PTO) and 1,1-dimethoxypropane (DMP) (Figure S1) in the EMC reaction. Most of other common oxides including TiO₂, WO₃, NiO, MoO₃, ZrO₂, SiO₂ and MgO used as support were sluggish (MP yield lower than 15%) (Table 1, entries 6–12). Efforts to optimize the catalysis of these oxides could not further increase the yield of MP. The

EMC reaction did not proceed over ceria support or in the absence of catalyst or CO (Table 1, entries 13–15). RuCl₃, the Ru precursor of Ru/ceria, yielded 16% MP even if extending the reaction time to 12 h (Table 1, entry 16). Ru supported on ceria with rod, cube and octahedron shapes were prepared and applied in the EMC reaction. All of them showed comparable activity (45–55% yield) to that of Ru/ceria (nanoparticle) (Table 1, entries 17–19). XRD did not identify Ru, inferring Ru is highly dispersed on ceria (Figure S2). We hereinafter employ Ru/ceria (nanoparticle) to study the reaction details of the EMC reaction.

Further optimization of the reaction conditions is conducted (Figure S3). A increase of CO partial pressure slightly affects the MP yield (~60%) (Figure S3A). The TOF reaches 8666 h⁻¹ at 1.0 MPa of CO in 8 h even if assuming all isolated Ru to be active sites. Even so, the TOF is about 2.5 times of Pd catalyst reported previously (~3500 h⁻¹).³⁴ Increase of reaction temperature leads to higher MP yield and the yield reaches 92% for 12 h at 165 °C (Figure S3B–C), the best result obtained in this study. Removal of the Ru/ceria catalyst in 1 h over the course of the reaction nearly stopped the conversion, and the MP yield leveled off at ~25%, indicating the reaction was heterogeneously catalyzed (Figure S4).

General Characterizations of Ru/Ceria. Figure 1 presents the results of a microstructural study of the Ru/ceria catalyst using electron microscopy. Because Ru and Ce have a similar atomic mass, HAADF-STEM images cannot provide enough contrast to visualize highly dispersed Ru on ceria. We here used STEM-EDX mapping to determine the distribution of Ce and Ru on this Ru/ceria sample. EDX mappings using the Ru L line reveal the presence of highly dispersed Ru clusters on ceria (see white arrows in Figure 1). Guided by EDX results, we are able to discern droplet-like oblate Ru clusters with an average size of about 1 nm on the ceria surface. Furthermore, it is observed that Ru clusters are preferentially located at defected sites like surface steps (see black arrows in Figure 1A and Figure 1C) or edges of the ceria substrate (Figure 1B–D). It is also observed that during TEM and STEM investigations under electron beam irradiation, the Ru clusters tend to be stuck at the surface defect sites (see Movie S1). Hereinafter, Ru/ceria is marked as Ru-clusters/ceria to highlight the unique property of ceria for the formation and stabilization of Ru clusters.

The Raman spectra indicate the presence of rich Vö and the Ru–O–Ce structure on Ru-clusters/ceria in comparison of pristine ceria support (Figure S5).^{10f,35} The formation of Ru–O–Ce linkage at the interface probably maintains the positively charged Ru species. More information on the Ru charge state is unraveled in Ru 3d spectra by in situ XPS (Figure 2). The

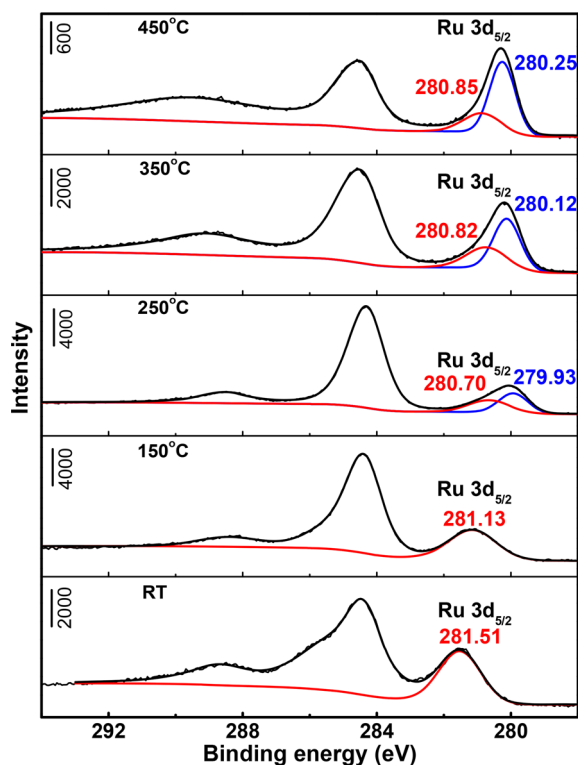


Figure 2. In situ XPS of Ru-clusters/ceria stepwise reduction at different temperatures ranging from room temperature to 450 °C.

signal of Ru 3d_{5/2} is often used for analyzing the charge state of the Ru species because another Ru 3d_{3/2} overlaps with C 1s at around 284.0 eV.³⁶ Prior to reduction, the Ru 3d_{5/2} at 281.51 eV is associated with Ru⁴⁺ in RuO₂.³⁷ The Ru⁰ starts to appear at 250 °C and gradually increase with increase of the reduction temperature, as indicated by the Ru 3d_{5/2} peak at 279.93 eV.³⁸ After reduction and formation of Ru^{δ+}, the peak shifts to 280.85 eV, and is still present up to 450 °C. The Ru^{δ+}/(Ru⁰ + Ru^{δ+}) ratios of Ru-clusters/ceria reduced at RT, 150, 250, 350 and 450 °C are calculated to be 1.00, 1.00, 0.47, 0.40, and 0.30 (Figure S6). In addition, the result of H₂-TPR suggests that the H₂ consumption of RuO₂/ceria is ~11.7 mmol·g_(RuO₂)⁻¹, which is lower than that of the stoichiometrically demanded H₂ consumption (~15.1 mmol·g_(RuO₂)⁻¹), confirming the presence of Ru^{δ+} under the harsh reducing condition (Figure S7).

XANES and EXAFS are applied to study the interface of Ru-clusters/ceria (Figure 3). The intensity of the white line reflects the Ru charge. The white line of Ru-clusters/ceria exhibits higher intensity than that of the Ru foil, indicating Ru in Ru-clusters/ceria is partly positively charged (Figure 3A), which is in agreement with the in situ XPS results. The spectra at the K-edge of Ru in k-space show that Ru-clusters/ceria is different to that of Ru foil (Figure 3B). Compared with the Ru foil, the peak intensity in the associated Fourier transforms of Ru-clusters/ceria is much weaker, demonstrating that Ru in Ru-clusters/ceria is highly dispersed (Figure 3C), which is in

agreement with the results of HAADF-STEM and EDX elemental mapping. The data-fitting results reveal that the coordination number (CN) of Ru from Ru–Ru bond in Ru-clusters/ceria is 2.4, which is much smaller than the coordination number of Ru foil (CN = 12), indicating that Ru is present as ultrasmall clusters in Ru-clusters/ceria (Figure 3D), which well correlates with the HRTEM and STEM/EDX results. Moreover, the fitting data also show Ru–Ru_{long} and Ru–Ce_{long} bond at the distance of 2.96 and 3.02 Å, respectively, which are both shorter than the bond length of Ru–Ru in RuO₂ (3.11 Å) but longer than that of the Ru foil (2.68 Å), which suggests that presence of partially oxidized Ru (Ru–Ru_{long}) and interfacial linkage Ru–O–Ce (Ru–Ce_{long}).³⁹

Activation of Ethylene, CO and Methanol from the In Situ IR. A series of in situ IR adsorption tests are employed to investigate the activation of ethylene, CO and methanol on Ru-clusters/ceria.

In situ IR spectra of **ethylene adsorption** on Ru-clusters/ceria presented a peak at 948 cm⁻¹ assigned to the ω(C–H) of chemically adsorbed ethylene (Figure 4A). The two peaks at 3081 and 2989 cm⁻¹ are assigned to ν_{as}(C–H) and ν_s(C–H) of the π-bounded ethylene (Figure 4B).⁴⁰ These peaks are still maintained even after desorption at 100 °C. The π-bounded adsorption mode of ethylene on Ru-clusters/ceria is also verified by ethylene-TPD test with an ethylene desorption peak ranging from 50 to 168 °C (Figure S8).⁴¹ For comparison, no obvious peak assigned to the chemically adsorbed ethylene is observed on pristine ceria (Figure S9), suggesting that the π-bounded ethylene on Ru-clusters/ceria is on Ru sites.⁴² For the adsorption of ethylene on Ru/silica, the π-bounded ethylene and the di-σ-bounded ethylene were found (Figure S10), suggesting the activity of Ru clusters for ethylene adsorption.

In situ Pyridine-IR spectra of **CO adsorption** on Ru-clusters/ceria showed three remarkable peaks at 2145 cm⁻¹, 2080 and 2008 cm⁻¹ (Figure 4C). The former two peaks are assigned to the multicarbonyl species on the partially oxidized Ru sites [Ru^{δ+}(CO)_x], although there is no consensus regarding the oxidation state of Ru (δ) and the number of carbonyl groups (x).⁴³ The later at 2008 cm⁻¹ is usually assigned to the linearly adsorbed CO on the low-coordinated Ru atoms on very small Ru particles.^{43a,b} For comparison, no obvious peaks assigned to the CO adsorption is observed on pristine ceria (Figure S11).

In situ IR spectra of **methanol adsorption** on pristine ceria indicated two peaks at 1101 and 1027 cm⁻¹ (Figure 4D), which are assigned to ν(C–O) of on-top and tridentate methoxy species, respectively.^{10f,44} The presence of tridentate methoxy species suggests that Vö is actually the active site for methanol dissociation.^{10f,44} In contrast, only 1010 cm⁻¹ peak is observed on Ru-clusters/ceria, which is assigned to ν(C–O) of tridentate methoxy species. Compared with that on pristine ceria, this peak is red-shifted significantly, indicating the higher content of Vö on Ru-clusters/ceria than pristine ceria after the induction of Ru to ceria.^{10f}

Interfacial Lewis Acid–Base Pair as Active Site for Methanol Dissociation and the Transfer of Hydrogen Species Verified by ¹H MAS NMR, In Situ IR and DFT Calculations. The generated methoxyl from the dissociation of methanol has been clearly detected by in situ IR. We turned to solid ¹H MAS NMR to detect the surface hydrogen species (Figure 5). This technique has been previously used for this purpose.⁴⁵ After methanol vapor pulse to Ru-clusters/ceria, two signals at 3.9 ppm and at 9.1 ppm are observed. The former is assigned to the methoxyl group, and the later to the hydroxyl

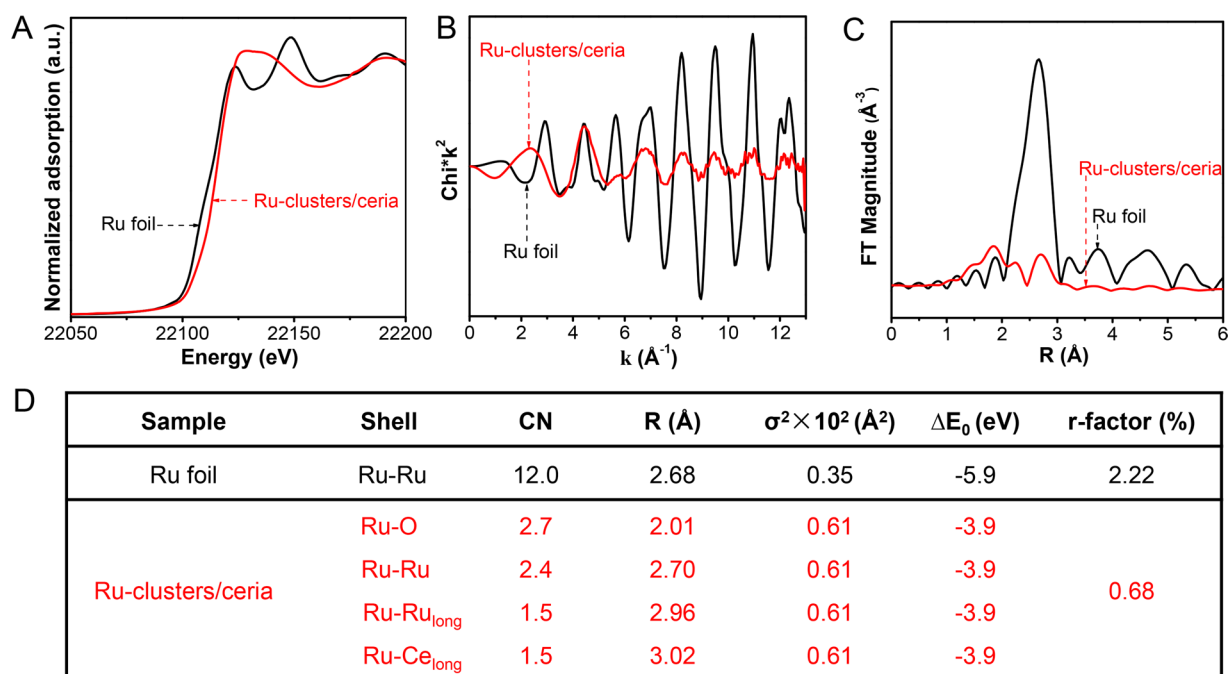


Figure 3. (A) The normalized XANES spectra at the Ru K-edge. (B) The k-space EXAFS spectra and (C) the corresponding Fourier transform of k^2 -weighted EXAFS spectra for a Ru foil and Ru-clusters/ceria. (D) EXAFS data fitting results of a Ru foil and Ru-clusters/ceria reduced at 350 °C. CN, the coordination number for the absorber-back scattering pair. R , the average absorber-back scattering distance. σ^2 , the Debye–Waller factor. ΔE_0 , the inner potential correction. The accuracies of the above parameters are estimated as CN, $\pm 20\%$; R , $\pm 1\%$; σ^2 , $\pm 20\%$; ΔE_0 , $\pm 20\%$.

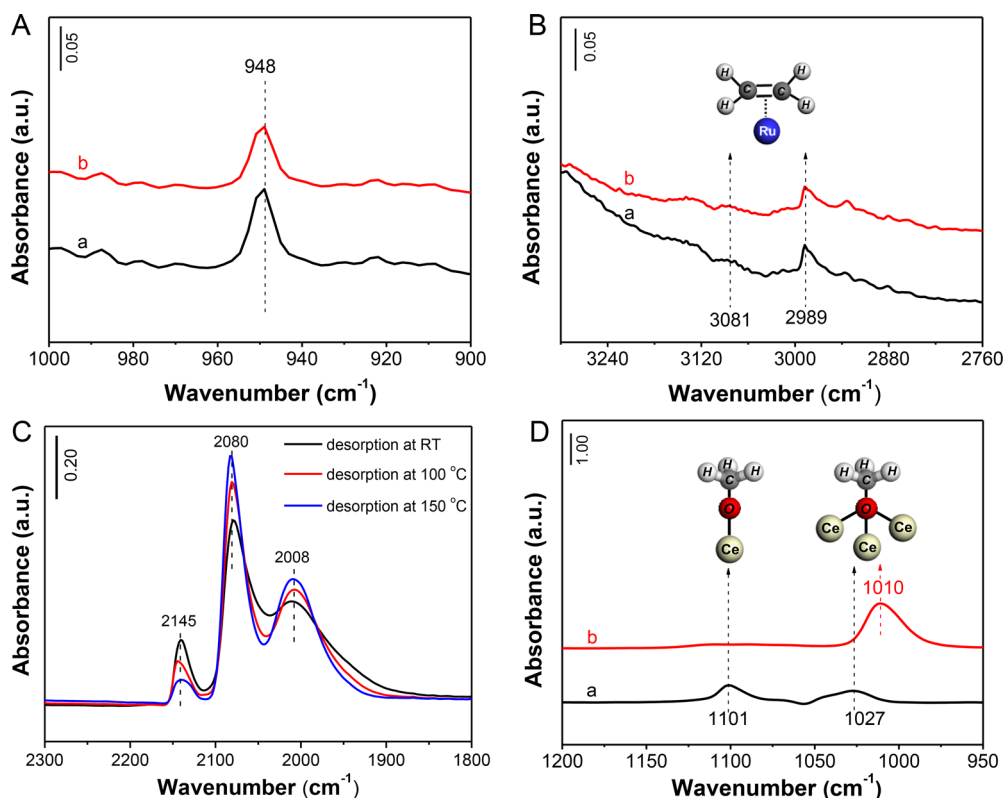


Figure 4. In situ IR of ethylene adsorption on Ru-clusters/ceria in the regions of (A) 1000–900 cm^{-1} and (B) 3300–2760 cm^{-1} . The spectra are collected after ethylene desorption at room temperature or at 100 °C in vacuum (less than 6×10^{-3} Pa). (C) IR spectra recorded after admission of CO and desorption at different temperatures (room temperature, 100 and 150 °C) on Ru-clusters/ceria. (D) In situ IR of methanol adsorption on ceria and (a) and Ru-clusters/ceria (b) in the region of 1200–950 cm^{-1} (less than 6×10^{-3} Pa).

formed via the transfer of hydrogen species to oxygen.⁴⁶ Followed by ethylene pulse, the later signal remarkably

decreases, but the signal at -0.04 ppm assigned to the ethyl group starts to appear,^{46b} indicating that the activated ethylene

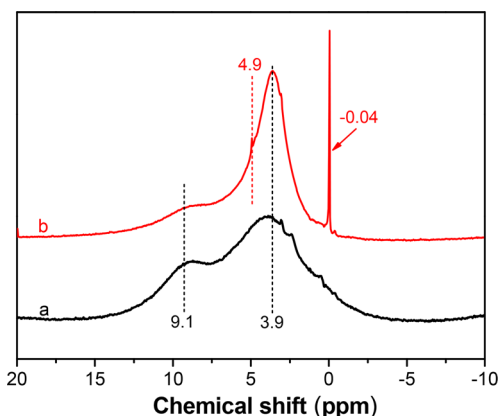


Figure 5. ^1H MAS NMR of (a) methanol and (b) ethylene after preadsorbed methanol on Ru-clusters/ceria.

is hydrogenated to ethyl group probably with hydroxyl group as hydrogen donor. In addition, a new signal at 4.9 ppm assigned to ethylene is also observed after the introduction of ethylene.

In situ pyridine-IR is conducted to detect the acidity with methanol preadsorption on Ru-clusters/ceria (Figure 6A). Several peaks are assigned to the adsorption of pyridine on Brønsted acid sites (1537 cm^{-1}), Lewis acid sites (1441 , 1570 , and 1602 cm^{-1}) and the overlapping of pyridine adsorption on Lewis and Brønsted acid sites (1486 cm^{-1}).⁴⁷ The intensities of these peaks decrease with increase of the desorption temperature. Most of pyridine desorbs from Brønsted acid sites at $350\text{ }^\circ\text{C}$, suggesting the moderate Brønsted acidity. In comparison, no obvious pyridine adsorption were observed on Ru-clusters/ceria without methanol preadsorption (Figure 6B), or on pristine ceria with methanol adsorbed (Figure S12). This infers that the active hydroxyl may be generated from the dissociation of methanol and located at the interface. Considering the function of Vö in the methanol dissociation, it becomes reasonable that the methanol dissociation at the interfacial Lewis acid–base pair (Ru–O–Ce–Vö) and the transfer of dissociated hydrogen are two primary steps in the acid-promoter-free EMC reaction. Raman spectra of the recovered catalyst after three times reaction which is less efficient indicate the shift of bands assigned to Ru–O–Ce and the weakening of Vö, suggesting the loss of interfacial acid–base pair sites. Again

it verifies the key role of such pair sites in the EMC reaction. (Figure S13).

The experimental results were then combined with theoretical calculations to explain the interfacial catalysis of Ru-clusters/ceria. An interfacial structure of Ru and ceria is created (Figure 7). First, the Bader charges of the Ru atoms at

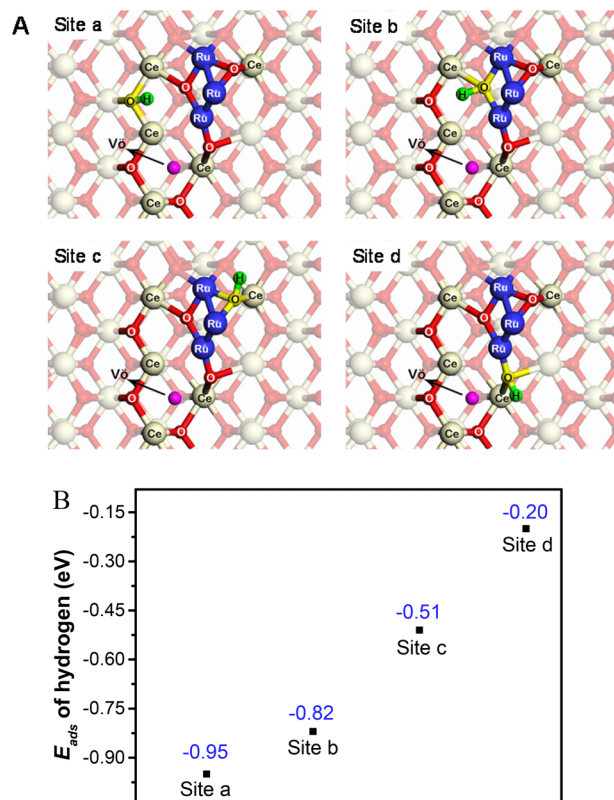


Figure 7. (A) The adsorption types of hydrogen on different oxygen sites (Site a, Site b, Site c, Site d) of Ru/CeO₂ (110). (B) The adsorption energy of hydrogen on different oxygen sites in Figure 7(A).

interface are calculated (Figure S14). It reveals the presence of the positively charged Ru, which consistent with the results of XPS and XANES. The adsorption energy of hydrogen on four

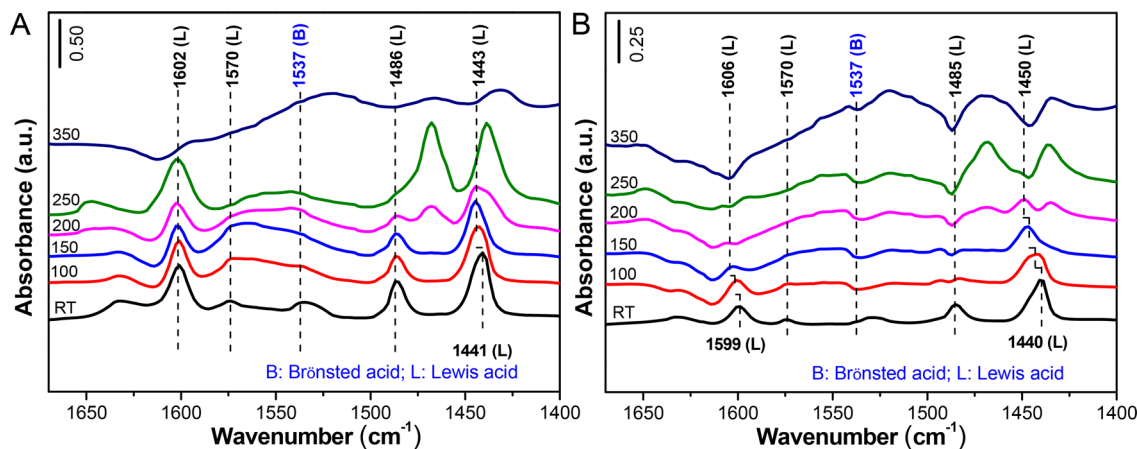


Figure 6. (A) In situ pyridine-IR of Ru-clusters/ceria with methanol preadsorption. (B) In situ pyridine-IR of the Ru-clusters/ceria without methanol preadsorption. The spectra are collected after ethylene desorption at different temperatures (room temperature, 100, 150, 200, 250 and $350\text{ }^\circ\text{C}$) in vacuum (less than $6 \times 10^{-3}\text{ Pa}$).

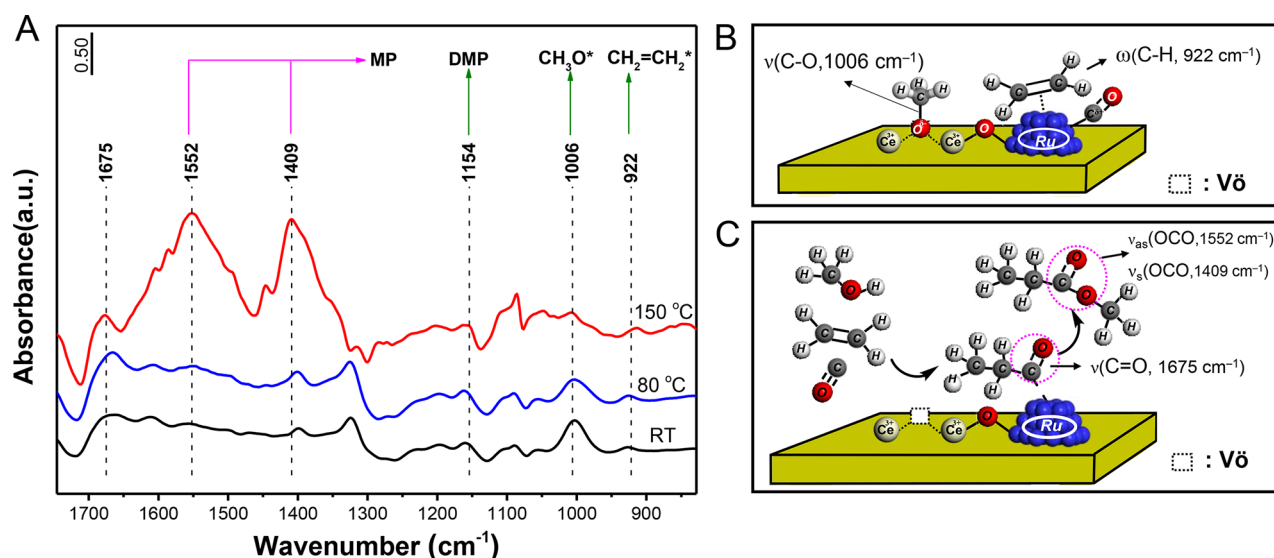


Figure 8. (A) In situ IR spectra for tracking the EMC reaction over Ru-clusters/ceria in the region of 1710–800 cm^{-1} . (B) The adsorption mode of methanol, ethylene and CO on Ru-clusters/ceria. (C) The intermediate and products observed in IR. MP, methyl propionate. DMP, 1,1-dimethoxypropane. ν_{as} , asymmetry stretching vibration. ν_{s} , symmetry stretching vibration. ω , wagging vibration.

kinds of oxygen are calculated (Figure 7A). It is found that the adsorption energy for hydrogen on [Ru-O-Ce-Vö] (Site d) is only -0.20 eV, which suggests the weakest binding between hydrogen and oxygen among the four types of oxygen sites which either locate at the interface without Vö in adjacent (Site b and Site c) or locate at CeO₂ surface (Site a) (Site a: -0.95 eV, Site b: -0.82 eV, Site c: -0.51 eV) (Figure 7B). The low adsorption energy makes the transfer of hydrogen located at [Ru-O-Ce-Vö] feasible to the Ru clusters.

The Reaction Details of Acid-Promoter-Free EMC Reaction. Identifying the possible reaction intermediates by IR was conducted (Figure 8A). The Ru-clusters/ceria catalyst was first saturated with ethylene, CO and methanol gas and then desorbed under vacuum at room temperature. After desorption, the peak at 922 cm^{-1} is assigned to the $\omega(\text{C-H})$ of π -bonded ethylene ($\text{CH}_2=\text{CH}_2^*$), while the peak at 1006 cm^{-1} to the $\nu(\text{C-O})$ of tridentate methoxy species (CH_3O^*) (Figure 8B). The target product MP appears when increasing the sample temperature to higher than 80 °C. The MP product features with the peaks at 1409 and 1552 cm^{-1} , ascribed to the $\nu_{\text{s}}(\text{O-C-O})$ and $\nu_{\text{as}}(\text{O-C-O})$ of MP, respectively.⁴⁸ The weak peak at 1154 cm^{-1} is assigned to the $\nu_{\text{as}}(\text{C-O-C})$ of 1,1-dimethoxypropane (DMP), a byproduct. Notably, a remarkable peak at 1675 cm^{-1} is observed, which can be attributed to the $\nu(\text{C=O})$ of the propionyl species ($\text{CH}_3\text{CH}_2\text{CO}^*$).⁴⁹ The propionyl species ($\text{CH}_3\text{CH}_2\text{CO}^*$) has been proved to be the intermediate in ethylene hydrogenation and hydroformylation reactions.⁵⁰ Here, assisted by in situ IR, the propionyl ($\text{CH}_3\text{CH}_2\text{CO}^*$) species is again confirmed to be a key intermediate in the EMC reaction.

On the basis of the above-mentioned results and the known chemistry of EMC reaction, we may generalize how the reaction takes place on Ru-clusters/ceria catalyst under acid-promoter-free conditions. Ethylene and CO are initially activated on Ru clusters. Methanol is activated on the Ce-Vö sites of Ru-O-Ce-Vö, generating tridentate methoxy species and active hydroxyl group [Ru-O(H)-Ce-Vö]. The active hydroxyls release protons to Ru clusters to attack the π -bonded ethylene on Ru-clusters, generating adsorbed ethyl (CH_3CH_2^*). The $\text{CH}_3\text{CH}_2\text{CO}^*$ intermediate is formed through the insertion of

activated CO to ethyl species. Finally, methoxyl (CH_3O^*) reacts with $\text{CH}_3\text{CH}_2\text{CO}^*$ species via a nucleophilic attack to give MP product and the active site is restored.

4. CONCLUSION

Despite of the complexity of the three-molecule-reaction, we have endeavored to classify the key role of the interface acid–base catalysis of Ru-clusters/ceria composite. We have employed structural, electronic and surface techniques (XRD, TEM, HAADF-STEM, EDX, Raman, XANES/EXAFS, TPR, TPD, and in situ experiments including XPS, IR and ¹H MAS NMR) to understand how the interfacial structure of the Ru-clusters/ceria affects the catalytic performance and to establish their relationship. Particularly we realize the first and successful example of the synthesis of methyl propionate from ethylene, CO and methanol via the EMC reaction with 92% MP yield without adding mineral acids. The catalyst also exhibits 2.5 times higher TOF value than the homogeneous Pd catalyst. We find the interfacial oxygen of Ru-O-Ce linkage at the interface of Ru-clusters/ceria together with adjacent Ce-Vö form a geometrically compatible Lewis acid–base pair sites [Ru-O-Ce-Vö]. The interfacial site [Ru-O-Ce-Vö] adsorbs and dissociates methanol, forming interfacial hydroxyl [Ru-O(H)-Ce-Vö] as acidic sites to react with ethylene. This explains why the present system does not require mineral acid additives. This work is not only fundamentally interesting but also practically meaningful.

■ ASSOCIATED CONTENT

Supporting Information

The Supporting Information containing is available free of charge via the Internet at The Supporting Information is available free of charge on the ACS Publications website at DOI: [10.1021/jacs.8b01742](https://doi.org/10.1021/jacs.8b01742).

General characterizations, GC, XRD, Raman, TPR, probe molecule-TPD, in situ IR spectra and reaction optimization experiments (PDF)

Movie S1 (AVI)

AUTHOR INFORMATION

Corresponding Author

*wangfeng@dicp.ac.cn

ORCID

Jianmin Lu: 0000-0003-3280-6466

Zhixin Zhang: 0000-0003-1321-5273

Xiaoyan Liu: 0000-0003-2694-2306

Tao Zhang: 0000-0001-9470-7215

Paolo Fornasiero: 0000-0003-1082-9157

Feng Wang: 0000-0002-9167-8743

Author Contributions

[†]J.A. and Y.W. contributed equally.

Notes

The authors declare no competing financial interest.

ACKNOWLEDGMENTS

This work was supported by the National Natural Science Foundation of China (21721004, 21690080, 21522608), Strategic Priority Research Program of the Chinese Academy of Sciences (XDB17020300), and Department of Science and Technology of Liaoning province (2015020086-101). Martin Gocyla and Marc Heggen thank the DFG for financial support within the grant HE 7192/1-1.

REFERENCES

- (1) (a) Zhao, G.; Yang, F.; Chen, Z.; Liu, Q.; Ji, Y.; Zhang, Y.; Niu, Z.; Mao, J.; Bao, X.; Hu, P.; Li, Y. *Nat. Commun.* **2017**, *8*, 14039. (b) Kropp, T.; Paier, J.; Sauer, J. *J. Am. Chem. Soc.* **2014**, *136*, 14616–14625.
- (2) (a) Li, W.; Huang, H.; Li, H.; Zhang, W.; Liu, H. *Langmuir* **2008**, *24*, 8358–8366. (b) Zorn, K.; Giorgio, S.; Halwax, E.; Henry, C. R.; Grönbeck, H.; Rupprechter, G. *J. Phys. Chem. C* **2011**, *115*, 1103–1111.
- (3) (a) Zhao, Y.; Cui, C.; Han, J.; Wang, H.; Zhu, X.; Ge, Q. *J. Am. Chem. Soc.* **2016**, *138*, 10191–10198. (b) Strayer, M. E.; Senftle, T. P.; Winterstein, J. P.; Vargas-Barbosa, N. M.; Sharma, R.; Rioux, R. M.; Janik, M. J.; Mallouk, T. E. *J. Am. Chem. Soc.* **2015**, *137*, 16216–16224. (c) Pham, T. N.; Sooknoi, T.; Crossley, S. P.; Resasco, D. E. *ACS Catal.* **2013**, *3*, 2456–2473. (d) Pappacena, A.; Rancan, M.; Armelao, L.; Llorca, J.; Ge, W.; Ye, B.; Lucotti, A.; Trovarelli, A.; Boaro, M. *J. Phys. Chem. C* **2017**, *121*, 17746–17755. (e) Sun, Q.; Wang, S.; Liu, H. *ACS Catal.* **2017**, *7*, 4265–4275. (f) Qu, J.; Zhou, X.; Xu, F.; Gong, X.-Q.; Tsang, S. C. E. *J. Phys. Chem. C* **2014**, *118*, 24452–24466.
- (4) (a) Liu, W.; Wang, W.; Tang, K.; Guo, J.; Ren, Y.; Wang, S.; Feng, L.; Yang, Y. *Catal. Sci. Technol.* **2016**, *6*, 2427–2434. (b) Singha, R. K.; Shukla, A.; Yadav, A.; Sivakumar Konathala, L. N.; Bal, R. *Appl. Catal., B* **2017**, *202*, 473–488. (c) Liu, Z.; Grinter, D. C.; Lustemberg, P. G.; Nguyen-Phan, T. D.; Zhou, Y.; Luo, S.; Waluyo, I.; Crumlin, E. J.; Stacchiola, D. J.; Zhou, J.; Carrasco, J.; Busnengo, H. F.; Ganduglia-Pirovano, M. V.; Senanayake, S. D.; Rodriguez, J. A. *Angew. Chem., Int. Ed.* **2016**, *55*, 7455–7459. (d) Zhu, J.; Giordano, L.; Lin, S.; Fang, Z.; Li, Y.; Huang, X.; Zhang, Y.; Pacchioni, G. *J. Phys. Chem. C* **2012**, *116*, 17668–17675. (e) Widmann, D.; Behm, R. J. *Chin. J. Catal.* **2016**, *37*, 1684–1693.
- (5) Chen, Z.; Mao, Y.; Chen, J.; Wang, H.; Li, Y.; Hu, P. *ACS Catal.* **2017**, *7*, 4281–4290.
- (6) (a) Carrasco, J.; Lopez-Duran, D.; Liu, Z.; Duchon, T.; Evans, J.; Senanayake, S. D.; Crumlin, E. J.; Matolin, V.; Rodriguez, J. A.; Ganduglia-Pirovano, M. V. *Angew. Chem., Int. Ed.* **2015**, *54*, 3917–3921. (b) Li, S.; Xu, Y.; Chen, Y.; Li, W.; Lin, L.; Li, M.; Dremg, Y.; Wang, X.; Ge, B.; Yang, C.; Yao, S.; Xie, J.; Li, Y.; Liu, X.; Ma, D. *Angew. Chem., Int. Ed.* **2017**, *56*, 10761–10765. (c) Gaudet, J. R.; de la Riva, A.; Peterson, E. J.; Bolin, T.; Datye, A. K. *ACS Catal.* **2013**, *3*, 846–855. (d) Pham, H. N.; Sattler, J. J.; Weckhuysen, B. M.; Datye, A. K. *ACS Catal.* **2016**, *6*, 2257–2264.
- (7) (a) Montini, T.; Melchionna, M.; Monai, M.; Fornasiero, P. *Chem. Rev.* **2016**, *116*, 5987–6041. (b) Vile, G.; Colussi, S.; Krumeich, F.; Trovarelli, A.; Perez-Ramirez, J. *Angew. Chem., Int. Ed.* **2014**, *53*, 12069–12072. (c) Rodriguez, J. A.; Grinter, D. C.; Liu, Z.; Palomino, R. M.; Senanayake, S. D. *Chem. Soc. Rev.* **2017**, *46*, 1824–1841. (d) Yashima, M. *Catal. Today* **2015**, *253*, 3–19. (e) Vivier, L.; Duprez, D. *ChemSusChem* **2010**, *3*, 654–678. (f) Mullins, D. R. *Surf. Sci. Rep.* **2015**, *70*, 42–85. (g) Paier, J.; Penschke, C.; Sauer, J. *Chem. Rev.* **2013**, *113*, 3949–3985.
- (8) (a) Wu, K.; Sun, L. D.; Yan, C. H. *Adv. Energy. Mater.* **2016**, *6*, 1600501. (b) Senanayake, S. D.; Stacchiola, D.; Rodriguez, J. A. *Acc. Chem. Res.* **2013**, *46*, 1702–1711. (c) Cargnello, M.; Grzelczak, M.; Rodriguez-Gonzalez, B.; Syrgiannis, Z.; Bakhmutsky, K.; La Parola, V.; Liz-Marzan, L. M.; Gorte, R. J.; Prato, M.; Fornasiero, P. *J. Am. Chem. Soc.* **2012**, *134*, 11760–11766.
- (9) (a) Cargnello, M.; Montini, T.; Polizzi, S.; Wieder, N. L.; Gorte, R. J.; Graziani, M.; Fornasiero, P. *Dalton Trans.* **2010**, *39*, 2122–2127. (b) Trovarelli, A.; Llorca, J. *ACS Catal.* **2017**, *7*, 4716–4735.
- (10) (a) Cargnello, M.; Doan-Nguyen, V. V. T.; Gordon, T. R.; Diaz, R. E.; Stach, E. A.; Gorte, R. J.; Fornasiero, P.; Murray, C. B. *Science* **2013**, *341*, 771–773. (b) Graciani, J.; Mudiyansele, K.; Xu, F.; Baber, A. E.; Evans, J.; Senanayake, S. D.; Stacchiola, D. J.; Liu, P.; Hrbek, J.; Sanz, J. F.; Rodriguez, J. A. *Science* **2014**, *345*, 546–550. (c) Jones, J.; Xiong, H.; DeLaRiva, A. T.; Peterson, E. J.; Pham, H.; Challa, S. R.; Qi, G.; Oh, S.; Wiebenga, M. H.; Pereira Hernández, X. I.; Wang, Y.; Datye, A. K. *Science* **2016**, *353*, 150–154. (d) Tamura, M.; Kitahara, T.; Nakagawa, Y.; Tomishige, K. *ACS Catal.* **2016**, *6*, 376–380. (e) Mitsudome, T.; Yamamoto, M.; Maeno, Z.; Mizugaki, T.; Jitsukawa, K.; Kaneda, K. *J. Am. Chem. Soc.* **2015**, *137*, 13452–13455. (f) Tamura, M.; Satsuma, A.; Shimizu, K.-i. *Catal. Sci. Technol.* **2013**, *3*, 1386–1393. (g) Yamada, Y.; Tsung, C. K.; Huang, W.; Huo, Z.; Habas, S. E.; Soejima, T.; Aliaga, C. E.; Somorjai, G. A.; Yang, P. *Nat. Chem.* **2011**, *3*, 372–376. (h) Barrabés, N.; Föttinger, K.; Llorca, J.; Dafinov, A.; Medina, F.; Sá, J.; Hardacre, C.; Rupprechter, G. *J. Phys. Chem. C* **2010**, *114*, 17675–17682. (i) Aneggi, E.; Wiater, D.; De Leitenburg, C.; Llorca, J.; Trovarelli, A. *ACS Catal.* **2014**, *4*, 172–181.
- (11) (a) Mao, M.; Lu, H.; Li, Y.; Yang, Y.; Zeng, M.; Li, N.; Zhao, X. *ACS Catal.* **2016**, *6*, 418–427. (b) Acerbi, N.; Tsang, S. C.; Jones, G.; Golunski, S.; Collier, P. *Angew. Chem., Int. Ed.* **2013**, *52*, 7737–41. (c) Deng, W.; Zhang, H.; Wu, X.; Li, R.; Zhang, Q.; Wang, Y. *Green Chem.* **2015**, *17*, S009–S018.
- (12) Kalck, P.; Urrutigoity, M. *Inorg. Chim. Acta* **2015**, *431*, 110–121.
- (13) Garcia-Suárez, E. J.; Khokarale, S. G.; van Buu, O. N.; Fehrmann, R.; Riisager, A. *Green Chem.* **2014**, *16*, 161–166.
- (14) Xiang, Y.; Zhou, J.; Lin, B.; Xue, X.; Tian, X.; Luo, Z. *Appl. Energy* **2015**, *157*, 499–507.
- (15) (a) Amadio, E.; Cavinato, G.; Härter, P.; Toniolo, L. *J. Organomet. Chem.* **2013**, *745*, 115–119. (b) Fanjul, T.; Eastham, G.; Haddow, M. F.; Hamilton, A.; Pringle, P. G.; Orpen, A. G.; Turner, T. P. W.; Waugh, M. *Catal. Sci. Technol.* **2012**, *2*, 937–950. (c) Ferreira, A. C.; Crous, R.; Bennie, L.; Meij, A. M.; Blann, K.; Bezuidenhout, B. C.; Young, D. A.; Green, M. J.; Roodt, A. *Angew. Chem., Int. Ed.* **2007**, *46*, 2273–2275. (d) De la Fuente, V.; Waugh, M.; Eastham, G. R.; Iggo, J. A.; Castillon, S.; Claver, C. *Chem. - Eur. J.* **2010**, *16*, 6919–6932. (e) Dong, K.; Fang, X.; Gulak, S.; Franke, R.; Spannenberg, A.; Neumann, H.; Jackstell, R.; Beller, M. *Nat. Commun.* **2017**, *8*, 14117.
- (16) (a) Gusev, O. V.; Kalsin, A. M.; Peterleitner, M. G.; Petrovskii, P. V.; Lyssenko, K. A.; Akhmedov, N. G.; Bianchini, C.; Meli, A.; Oberhauser, W. *Organometallics* **2002**, *21*, 3637–3649. (b) Bianchini, C.; Meli, A.; Oberhauser, W.; Zuideveld, M. A.; Freixa, Z.; Kamer, P. C. J.; Spek, A. L.; Gusev, O. V.; Kal'sin, A. M. *Organometallics* **2003**, *22*, 2409–2421.
- (17) (a) Dong, K.; Sang, R.; Fang, X.; Franke, R.; Spannenberg, A.; Neumann, H.; Jackstell, R.; Beller, M. *Angew. Chem., Int. Ed.* **2017**, *56*, 5267–5271. (b) Li, H.; Dong, K.; Jiao, H.; Neumann, H.; Jackstell, R.; Beller, M. *Nat. Chem.* **2016**, *8*, 1159–1166.
- (18) Blanco, C.; Godard, C.; Zangrando, E.; Ruiz, A.; Claver, C. *Dalton Trans.* **2012**, *41*, 6980–6991.

- (19) (a) Zhang, Z.; Wang, Y.; Wang, M.; Lu, J.; Li, L.; Zhang, Z.; Li, M.; Jiang, J.; Wang, F. *Chin. J. Catal.* **2015**, *36*, 1623–1630. (b) Zhang, Z.; Wang, Y.; Wang, M.; Lu, J.; Zhang, C.; Li, L.; Jiang, J.; Wang, F. *Catal. Sci. Technol.* **2016**, *6*, 1693–1700.
- (20) (a) Mai, H. X.; Sun, L. D.; Zhang, Y. W.; Si, R.; Feng, W.; Zhang, H. P.; Liu, H. C.; Yan, C. H. *J. Phys. Chem. B* **2005**, *109*, 24380–24385. (b) Wang, Y.; Wang, F.; Song, Q.; Xin, Q.; Xu, S.; Xu, J. *J. Am. Chem. Soc.* **2013**, *135*, 1506–1515.
- (21) It should be handled inside a well-ventilated hood to avoid inhalation. Additionally, a CO sensor should be installed around the bench.
- (22) Kovács, A.; Schierholz, R.; Tillmann, K. *JLSRF* **2016**, *2*, 43.
- (23) Thust, A.; Barthel, J.; Tillmann, K. *JLSRF* **2016**, *2*, 41.
- (24) Boudeville, Y.; Figueras, F.; Forissier, M.; Portefaix, J. L.; Vedrine, J. C. *J. Catal.* **1979**, *58*, 52–60.
- (25) Scofield, J. H. *J. Electron Spectrosc. Relat. Phenom.* **1976**, *8*, 129–137.
- (26) Kresse, G.; Furthmüller, J. *Comput. Mater. Sci.* **1996**, *6*, 15–50.
- (27) Perdew, J. P.; Burke, K.; Ernzerhof, M. *Phys. Rev. Lett.* **1996**, *77*, 3865–3868.
- (28) Kresse, G.; Joubert, D. *Phys. Rev. B: Condens. Matter Mater. Phys.* **1999**, *59*, 1758–1775.
- (29) Grimme, S.; Antony, J.; Ehrlich, S.; Krieg, H. *J. Chem. Phys.* **2010**, *132*, 154104.
- (30) Henkelman, G.; Uberuaga, B. P.; Jonsson, H. *J. Chem. Phys.* **2000**, *113*, 9901–9904.
- (31) (a) Henkelman, G.; Jonsson, H. *J. Chem. Phys.* **1999**, *111*, 7010–7022. (b) Heyden, A.; Bell, A. T.; Keil, F. J. *J. Chem. Phys.* **2005**, *123*, 224101. (c) Olsen, R. A.; Kroes, G. J.; Henkelman, G.; Arnaldsson, A.; Jonsson, H. *J. Chem. Phys.* **2004**, *121*, 9776–9792.
- (32) Wang, Y.; Zhang, J.; Chen, H.; Zhang, Z.; Zhang, C.; Li, M.; Wang, F. *Green Chem.* **2017**, *19*, 88–92.
- (33) (a) Ostrom, H.; Oberg, H.; Xin, H.; Larue, J.; Beye, M.; Dell'Angela, M.; Gladh, J.; Ng, M. L.; Sellberg, J. A.; Kaya, S.; Mercurio, G.; Nordlund, D.; Hantschmann, M.; Hieke, F.; Kuhn, D.; Schlotter, W. F.; Dakovski, G. L.; Turner, J. J.; Minitti, M. P.; Mitra, A.; Moeller, S. P.; Fohlich, A.; Wolf, M.; Wurth, W.; Persson, M.; Norskov, J. K.; Abild-Pedersen, F.; Ogasawara, H.; Pettersson, L. G. M.; Nilsson, A. *Science* **2015**, *347*, 978–982. (b) Huang, B.; Kobayashi, H.; Yamamoto, T.; Matsumura, S.; Nishida, Y.; Sato, K.; Nagaoka, K.; Kawaguchi, S.; Kubota, Y.; Kitagawa, H. *J. Am. Chem. Soc.* **2017**, *139*, 4643–4646.
- (34) Abe, T.; Tanizawa, M.; Watanabe, K.; Taguchi, A. *Energy Environ. Sci.* **2009**, *2*, 315–321.
- (35) Lin, W.; Herzing, A. A.; Kiely, C. J.; Wachs, I. E. *J. Phys. Chem. C* **2008**, *112*, 5942–5951.
- (36) (a) Wang, R.; Wang, Y.; Ren, M.; Sun, G.; Gao, D.; Chin Chong, Y. R.; Li, X.; Chen, G. *Int. J. Hydrogen Energy* **2017**, *42*, 6757–6764. (b) Wang, F.; Li, C.; Zhang, X.; Wei, M.; Evans, D. G.; Duan, X. *J. Catal.* **2015**, *329*, 177–186.
- (37) (a) Soin, N.; Roy, S. S.; Mitra, S. K.; Thundat, T.; McLaughlin, J. A. *J. Mater. Chem.* **2012**, *22*, 14944–14950. (b) Singh, P.; Hegde, M. S. *Chem. Mater.* **2009**, *21*, 3337–3345.
- (38) Ye, X. R.; Lin, Y. H.; Wang, C. M.; Engelhard, M. H.; Wang, Y.; Wai, C. M. *J. Mater. Chem.* **2004**, *14*, 908–913.
- (39) (a) Farmer, J. A.; Campbell, C. T. *Science* **2010**, *329*, 933–936. (b) Esch, F.; Fabris, S.; Zhou, L.; Montini, T.; Africh, C.; Fornasiero, P.; Comelli, G.; Rosei, R. *Science* **2005**, *309*, 752–755. (c) Cargnello, M.; Jaen, J. J. D.; Garrido, J. C. H.; Bakhmutsky, K.; Montini, T.; Gamez, J. J. C.; Gorte, R. J.; Fornasiero, P. *Science* **2012**, *337*, 713–717.
- (40) (a) Jimenez Orozco, C.; Florez, E.; Moreno, A.; Liu, P.; Rodriguez, J. A. *J. Phys. Chem. C* **2016**, *120*, 13531–13540. (b) Heard, C. J.; Hu, C.; Skoglundh, M.; Creaser, D.; Grönbeck, H. *ACS Catal.* **2016**, *6*, 3277–3286. (c) Kravchuk, T.; Venugopal, V.; Vattuone, L.; Burkholder, L.; Tyssoe, W. T.; Smerieri, M.; Rocca, M. *J. Phys. Chem. C* **2009**, *113*, 20881–20889. (d) Rioux, R. M.; Hoefelmeyer, J. D.; Grass, M.; Song, H.; Niesz, K.; Yang, P.; Somorjai, G. A. *Langmuir* **2008**, *24*, 198–207. (e) Parlett, P. M.; Chesters, M. A. *Surf. Sci.* **1996**, *357*, 791–795.
- (41) (a) Chen, Y.; Chen, J. *Appl. Surf. Sci.* **2016**, *387*, 16–27. (b) Kim, E.; Shin, E. W.; Bark, C. W.; Chang, I.; Yoon, W. J.; Kim, W. *J. Appl. Catal., A* **2014**, *471*, 80–83.
- (42) Heard, C. J.; Siahrostami, S.; Grönbeck, H. *J. Phys. Chem. C* **2016**, *120*, 995–1003.
- (43) (a) Kantcheva, M.; Sayan, S. *Catal. Lett.* **1999**, *60*, 27–38. (b) Chin, S. Y.; Williams, C. T.; Amiridis, M. D. *J. Phys. Chem. B* **2006**, *110*, 871–882. (c) Hadjiivanov, K.; Lavalley, J. C.; Lamotte, J.; Mauge, F.; Saint-Just, J.; Che, M. *J. Catal.* **1998**, *176*, 415–425.
- (44) (a) Wu, Z.; Li, M.; Mullins, D. R.; Overbury, S. H. *ACS Catal.* **2012**, *2*, 2224–2234. (b) D'Angelo, A. M.; Wu, Z.; Overbury, S. H.; Chaffee, A. L. *J. Phys. Chem. C* **2016**, *120*, 27996–28008.
- (45) Zhang, W. P.; Xu, S. T.; Han, X. W.; Bao, X. H. *Chem. Soc. Rev.* **2012**, *41*, 192–210.
- (46) (a) Anderson, M. W.; Klinowski, J. *J. Am. Chem. Soc.* **1990**, *112*, 10–16. (b) Mastikhin, V. M.; Mudrakovsky, I. L.; Nosov, A. V. *Prog. Nucl. Magn. Reson. Spectrosc.* **1991**, *23*, 259–299.
- (47) Zhang, Z.; Wang, Y.; Lu, J.; Zhang, C.; Wang, M.; Li, M.; Liu, X.; Wang, F. *ACS Catal.* **2016**, *6*, 8248–8254.
- (48) Ferencz, Z.; Erdőhelyi, A.; Baán, K.; Oszkó, A.; Óvári, L.; Kónya, Z.; Papp, C.; Steinrück, H. P.; Kiss, J. *ACS Catal.* **2014**, *4*, 1205–1218.
- (49) (a) Sivasankar, N.; Frei, H. *J. Phys. Chem. C* **2011**, *115*, 7545–7553. (b) Huang, L.; Xu, Y. *Catal. Lett.* **2000**, *69*, 145–151. (c) Pien, S. I.; Chuang, S. S. C. *J. Mol. Catal.* **1991**, *68*, 313–330.
- (50) Wasylenko, W.; Frei, H. *J. Phys. Chem. B* **2005**, *109*, 16873–16878.